

Cite this: *Dalton Trans.*, 2021, **50**, 1106

On the non-innocence and reactive *versus* non-reactive nature of α -diketones in a set of diruthenium frameworks†

Farheen Fatima Khan,^a Saikat Mondal,^a Shubhadeep Chandra,^b Nicolas I. Neuman,^b Biprajit Sarkar^b and Goutam Kumar Lahiri^b *^a

α -Diketones are an important class of building blocks employed in many organic synthetic reactions. However, their coordination chemistry has rarely been explored. In light of this, our earlier report on [(acac)₂Ru^{II}(μ -2,2'-pyridil)Ru^{II}(acac)₂] (acac = acetylacetonate) showcased the sensitivity of a diketone fragment towards oxidative C–C cleavage. Following the lead, the synthesis of similar but stable diketone fragments containing diruthenium compounds was attempted. Three diruthenium compounds with the bridge 1,2-bis(2-hydroxyphenyl)ethane-1,2-dione (L) were prepared: diastereomeric [(acac)₂Ru^{III}(μ -L²⁻)Ru^{III}(acac)₂], **1a**(*rac*)/**1b**(*meso*), [(bpy)₂Ru^{II}(μ -L²⁻)Ru^{II}(bpy)₂](ClO₄)₂, [**2**](ClO₄)₂ and [(pap)₂Ru^{II}(μ -L²⁻)Ru^{II}(pap)₂](ClO₄)₂, [**3**](ClO₄)₂ with ancillary ligands of different donating/accepting characteristics. The metal is stabilised in different oxidation states in these complexes: Ru(III) is preferred in **1a/1b** when σ -donating acac is used as the co-ligand whereas electron rich Ru(II) is preferred in [**2**](ClO₄)₂ and [**3**](ClO₄)₂ when co-ligands of moderate to strong π -accepting properties are employed. The oxidative chemistry of these systems is of particular interest with respect to the participation of varying bridging-ligands which contain phenoxide groups. On the other hand, the reduction processes primarily resulting from the metal or the ancillary ligands are noteworthy as the normally reducible 1,2-diketo- group remains unreduced. These results have been rationalised and outlined from thorough experimental and theoretical investigations. The results presented here shed light on the stability of metal coordinated α -diketones as a function of their substituents.

Received 1st October 2020,
Accepted 3rd December 2020

DOI: 10.1039/d0dt03400b

rsc.li/dalton

Introduction

Quinones are a class of oxidised aromatics that are indispensably pivotal in the aerobic metabolism of cells and are constituents of a variety of enzymes.¹ This class of organic functionalities is frequently researched due to their well-established capability of sequential one electron transfer events which allow access to singly reduced semiquinone and doubly reduced catecholate forms.² Nature often takes advantage of

these electron shuttles in the functioning of metalloenzymes, which usually occurs through inner sphere electron transfer in the catalytic processes of enzymes.³ In recent years, our group has extensively explored quinone type ligands for studying various electron transfer aspects and ligand assisted transformations that encompass biological and fundamental interests.⁴ A recent report from our group in this regard inspected the electronic aspects of *ortho*-quinone type 2,2'-pyridil with the Ru(acac)₂ (acac = acetylacetonate) metal fragment and its consecutive ligand assisted reactivity leading to dioxygen activation followed by C–C cleavage (Fig. 1).⁵

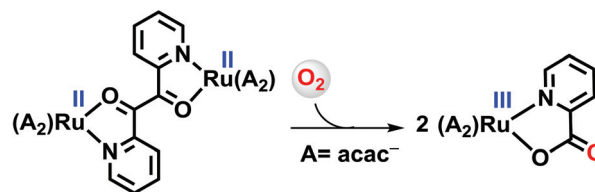


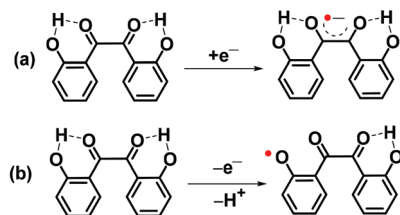
Fig. 1 Previous report from the group depicting C–C cleavage in the diruthenium complexes of 2,2'-pyridil.⁵

^aDepartment of Chemistry, Indian Institute of Technology Bombay, Powai, Mumbai-400076, India. E-mail: lahiri@chem.iitb.ac.in

^bLehrstuhl für Anorganische Koordinationschemie, Institut für Anorganische Chemie, Universität Stuttgart, Pfaffenwaldring 55, D-70550 Stuttgart, Germany.

E-mail: biprajit.sarkar@iac.uni-stuttgart.de

† Electronic supplementary information (ESI) available: X-ray crystallographic files in CIF format for [**2**](ClO₄)₂ and [**3**](ClO₄)₂, mass spectra (Fig. S1), ¹H NMR (Fig. S2), DFT optimised structures (Fig. S3), crystallographic and DFT calculated bond parameters (Tables S1–S7), MO compositions (Tables S8–S22), energies of optimised structures (Table S23) and TD-DFT (Table S24) (PDF). CCDC 2026821 ([**2**](ClO₄)₂) and 2026822 ([**3**](ClO₄)₂), contain the supplementary crystallographic data for this paper. For ESI and crystallographic data in CIF or other electronic format see DOI: 10.1039/D0DT03400B



Scheme 1 (a) Reduction and (b) oxidation possibilities for L.

The observation of such dioxygen driven cleavage activity in 2,2'-pyridil obviously raises the question of the generality of such C–C bond cleavage reactions in related diketo-containing compounds. In this work, the stability/instability of 1,2-bis(2-hydroxyphenyl) ethane-1,2-dione (L)⁶ (Scheme 1), a symmetrical bridging ligand composed of a mixed donor (redox active phenoxide, upon deprotonation)–acceptor (keto groups) system, and its activity/inactivity towards dioxygen are investigated in a set of ruthenium complexes.

The ligand (L) can in principle exhibit the following electronic forms as shown in Scheme 1: (a) the $L^{\cdot-}$ form upon reduction and the electron being accommodated at the diketo unit⁷ and (b) the $L^{\cdot+}$ form upon oxidation where the oxidation may be found to take place at the phenol unit.

While the deprotonated phenols have been established in their commonly observed phenoxide form, their uncommon oxidised forms, phenoxyl radical and phenoxium cation, have also been documented.⁸ Such processes are of interest since many metalloenzymes like galactose oxidase contain a tyrosinyl radical and such radical systems are known to be stabilised by metal coordination.⁹

Herein, we report the syntheses, characterisation, and experimental and theoretical evaluation of the diruthenium complexes **1a/1b**, $[2](\text{ClO}_4)_2$ and $[3](\text{ClO}_4)_2$ (Fig. 2). We also address the stability/reactivity of 2,2'-pyridil *versus* L in the corresponding ruthenium complexes, and provide a rationale for the experimental observations (Fig. 1).

Results and discussion

Syntheses, characterisation and molecular structures

The dinuclear complexes **1a/1b**, $[2](\text{ClO}_4)_2$ and $[3](\text{ClO}_4)_2$ were prepared by following the protocols developed earlier^{Ab-d} for the synthesis of a variety of diruthenium complexes. The reaction of 1,2-bis(2-hydroxyphenyl)ethane-1,2-dione (L) and the precursor complex $\text{Ru}^{\text{II}}(\text{acac})_2(\text{CH}_3\text{CN})_2$ in refluxing toluene in the presence of NEt_3 as a base under a dinitrogen atmosphere followed by chromatographic separation generated paramagnetic diastereomers $[(\text{acac})_2\text{Ru}^{\text{III}}(\mu\text{-L}^{\cdot-})\text{Ru}^{\text{III}}(\text{acac})_2]$, **1a** (*rac*($\Delta\Delta/\Lambda\Lambda$)) and **1b** (*meso*($\Delta\Lambda$)) due to the presence of two chiral metal centres.⁵ The corresponding diamagnetic complexes $[(\text{bpy})_2\text{Ru}^{\text{II}}(\mu\text{-L}^{\cdot-})\text{Ru}^{\text{II}}(\text{bpy})_2](\text{ClO}_4)_2$, $[2](\text{ClO}_4)_2$ and $[(\text{pap})_2\text{Ru}^{\text{II}}(\mu\text{-L}^{\cdot-})\text{Ru}^{\text{II}}(\text{pap})_2](\text{ClO}_4)_2$, $[3](\text{ClO}_4)_2$ were prepared from *in situ* generated *cis*- $[\text{Ru}(\text{bpy})_2(\text{EtOH})_2]^{2+}$ and *ctc*- $[\text{Ru}(\text{pap})_2(\text{EtOH})_2]^{2+}$, respectively, and R (bpy = 2,2'-bipyridine, pap = 2-phenylazopyridine, and *ctc* = *cis-trans-cis* configuration with respect to EtOH, pyridine, and azo nitrogen donors of pap ligands, respectively¹⁰) and L in the presence of NEt_3 base in refluxing toluene followed by chromatographic purification on a neutral alumina column. As is not uncommon, due to the concurring stabilisation of the high valent Ru^{III} ¹¹ state in the complexes **1a/1b** and that of Ru^{II} in $[2](\text{ClO}_4)_2/[3](\text{ClO}_4)_2$ due to the effects of the dianionic bridge, the σ -donating nature of the acac ancillary fragment and the π -accepting nature of the bpy/pap co-ligands,¹² respectively, have been observed and established (*vide infra*).

The electrically neutral **1a/1b** and 1 : 2 conducting $[2](\text{ClO}_4)_2$ and $[3](\text{ClO}_4)_2$ compounds were subjected to multiple characterisation techniques and they yielded satisfactory micro-analytical and mass data (Experimental section and Fig. S1†).

The appearance of the forbidden half-field signals¹³ along with anisotropic (rhombic) EPR (Fig. 3) at 100 K for **1a/1b** affirmed the presence of two metal-centred spins which contribute to the triplet ($\text{Ru}^{\text{III}}(t_{2g}^5)\text{-Ru}^{\text{III}}(t_{2g}^5)$) spin state ($S = 1$) in these complexes.

The characteristic paramagnetic contact shifted¹⁴ $^1\text{H-NMR}$ resonances corresponding to full and half molecules over a wide chemical shift range from 20 ppm to -30 ppm approxi-

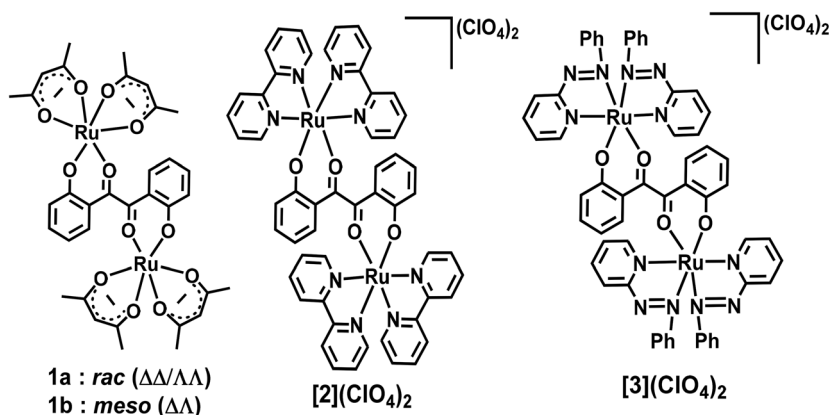


Fig. 2 Representation of the complexes.

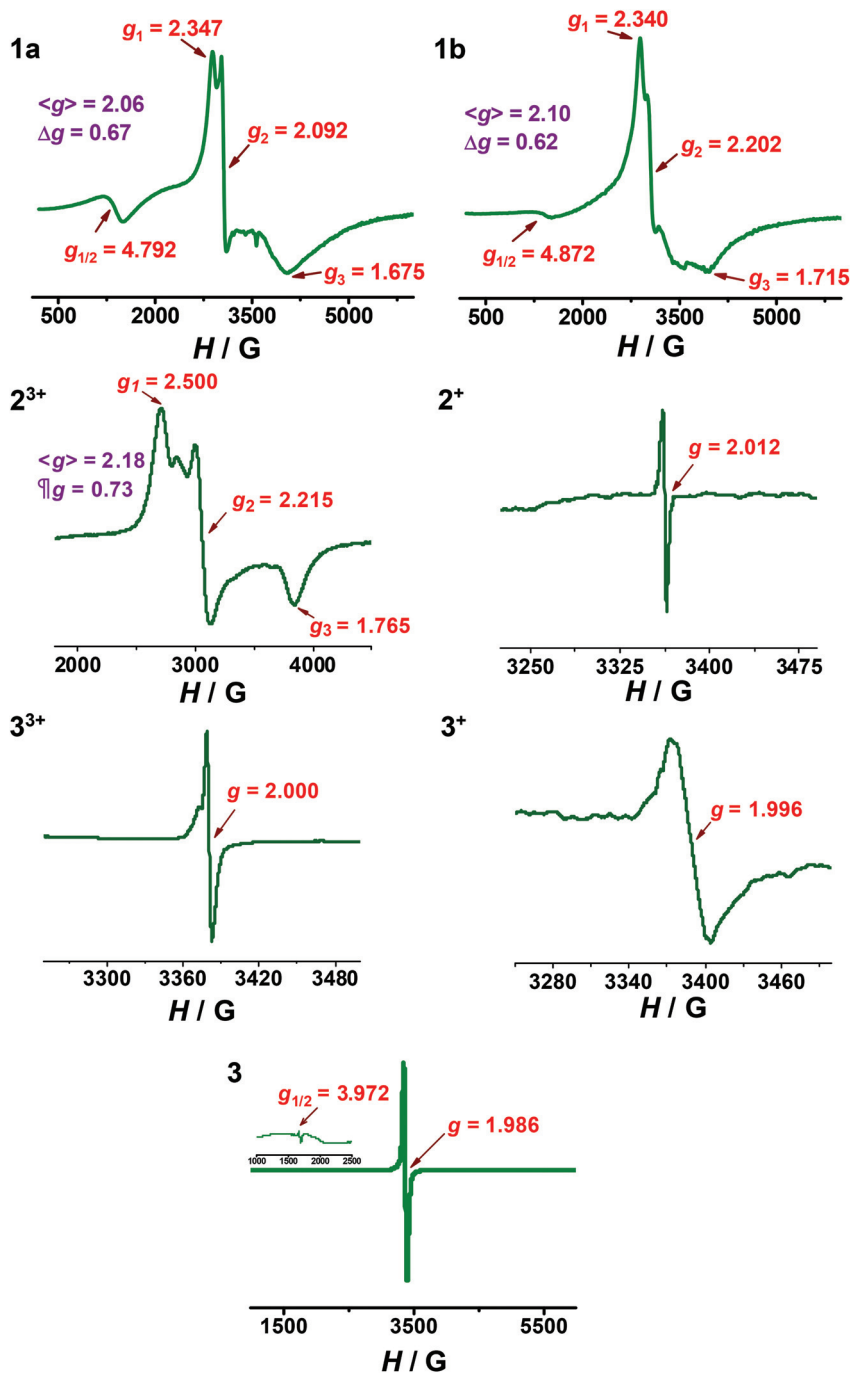


Fig. 3 X-band EPR spectra in a $\text{CH}_2\text{Cl}_2/\text{toluene}$ (1 : 2) mixture at 5 K.

mately for the diastereomeric pair **1a** and **1b**, respectively, further establish the presence of unpaired electron spins (Fig. S2†). Multiple overlapping proton resonances corresponding to the full molecule and half molecule were observed in the aromatic chemical shift range for diamagnetic $[\text{2}](\text{ClO}_4)_2$ and $[\text{3}](\text{ClO}_4)_2$ (Fig. S2†), respectively, as could also be corroborated from their single crystal X-structures (Fig. 4).

Several attempts towards the crystallisation of the diastereomeric pair unfortunately only led to the formation of very thin

and fragile crystals that did not diffract. However, the successful diffraction of single crystals of $[\text{2}](\text{ClO}_4)_2$ and $[\text{3}](\text{ClO}_4)_2$ helped in gaining insights into the structural and electronic details of these complexes. The structural parameters could largely be approximated and reproduced by theoretical calculations (Fig. 4, Fig. S3 and Tables S1–S7†).

Considering the various probabilities around the dinuclear chelation with the tetradentate ligand **L**, which here acts as a bis-bidentate chelating ligand, an outlining sketch may be

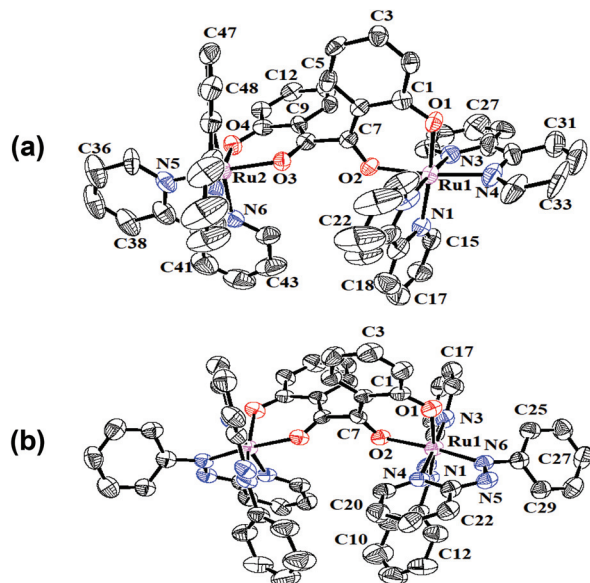


Fig. 4 Perspective views of the cations (a) $[2](\text{ClO}_4)_2$ and (b) $[3](\text{ClO}_4)_2$. Ellipsoids are drawn at 50% probability levels. Hydrogen atoms and perchlorates are removed for clarity.

referenced from Fig. 5. The possibilities **a** and **b** are less likely, and since the crystal structure shows six-membered chelates, these are ruled out as a major isolable fraction of the reaction mixture. This may be rationalised due to the strong preference of the formation of six-membered over seven or higher-membered ring chelates due to the stability reasons. The **c** and **d** forms present may be recognised as two distinct extremes of *cis*- and *trans*- forms which are likely but the adoption of a *cis*-type configuration would be sterically demanding owing to the presence of spatially encumbered metal centres with two ancillary fragments and similarly a strict *trans*- form would be difficult to attain due to repulsions that may arise between the pendant phenyl rings of the ligand and the neighbouring ancillary groups. Thus, the molecular structures (Fig. 4) of the complexes $[2](\text{ClO}_4)_2$ and $[3](\text{ClO}_4)_2$ nearly display a configuration that is rather an intermediate of the *cis*- and *trans*- forms with the angles between the two chelate rings being 82.87° and 84.56° , respectively, for the bis-chelated complexes. The geometry around each metal centre is pseudo octahedral as it is commonly observed due to the differing chelating environment extended by the bridging ligand, the co-ligands and their different donor atoms.¹⁵ The metrical parameter involving C=O

bond lengths of $1.274(9)$ Å and $1.263(8)$ Å for $[2](\text{ClO}_4)_2$ and $[3](\text{ClO}_4)_2$, respectively, is suggestive of the presence of an unreduced coordinated carbonyl function and similar conclusions for complex **1** may also be drawn from the computational values (Tables S2, S4 and S6†). The average azo bond distance of pap in $[3](\text{ClO}_4)_2$ of $1.291(7)$ Å also reflects its unreduced state.^{10b}

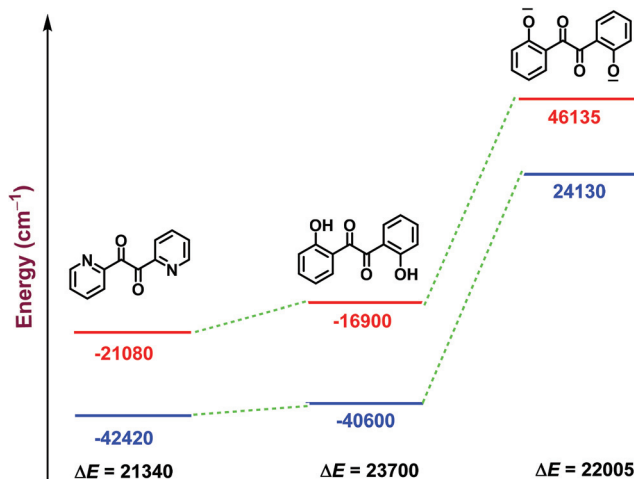


Fig. 6 Comparative energy levels of free ligands. Blue and red lines represent the HOMO and LUMO levels, respectively. $\Delta E = \text{HOMO} - \text{LUMO}$ gap.

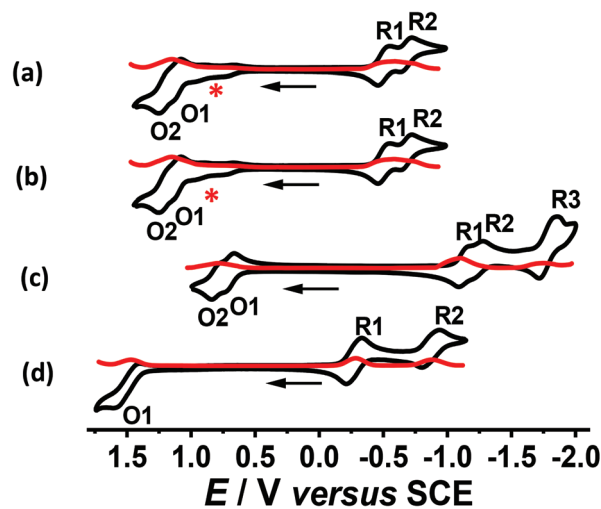


Fig. 7 Cyclic and differential pulse voltammograms for (a) **1a**, (b) **1b**, (c) $[2](\text{ClO}_4)_2$ and (d) $[3](\text{ClO}_4)_2$ in CH_3CN .

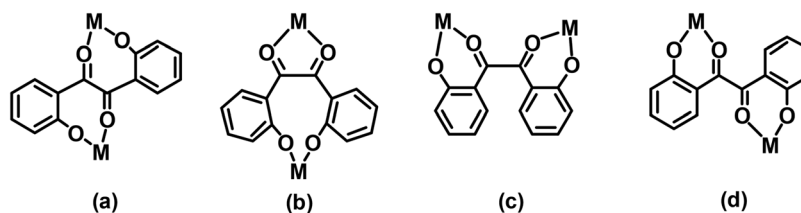


Fig. 5 Probable binding modes of L in a dinuclear framework.

Rationale for the stability of the complexes

It can be seen from the above discussion that deprotonated 1,2-bis(2-hydroxyphenyl)ethane-1,2-dione (L) binds to the metal ions and remains stable and intact upon metallation. Initially the ligand was screened with the {Ru(acac)₂} framework for stability. Upon obtaining stable complex **1**, the ligand was further explored in the diruthenium complexes having varying electronic features of the ancillary ligands by employing {Ru(bpy)₂} and {Ru(pap)₂} metal fragments and interestingly that also led to the stable complexes [2](ClO₄)₂ and [3](ClO₄)₂, respectively. These results are strikingly different from those of the corresponding 2,2'-pyridil containing complexes in which the fragile 1,2-diketo fragment cleaves at the C-C bond upon exposure to air.⁵ Intrigued by the sensitivity of the diketo fragment in 2,2'-pyridil which was proposed to be majorly activated by redox tautomerism, we therefore chose L to affirm the mechanistic outlines reported earlier – by eliminating the possibility of redox tautomerism that should ultimately lead to stable complexes with an intact diketo moiety.

Gratifyingly, the replacement of the pyridine ring in 2,2'-pyridil with a phenolic group in L indeed gave us access to air stable complexes **1**-[2](ClO₄)₂/[3](ClO₄)₂ even when the metal centre bore different electronic environments around it. These successful results could be justified by the following two reasons: (i) the elimination of the probability of the formation of a redox tautomer and (ii) an increase in the energy of the ligand LUMO upon moving the electronegative group away from the pendant ring and an overall increase of the electron density in its deprotonated form as can be visualised from the DFT calculated energy comparison diagram (Fig. 6). The latter also strengthens the prior study.

Furthermore, attempts towards small molecule activation (O₂) by the chemical reduction of the bridge (L) in the complexes were also not successful. This could also be compre-

hended on the same lines that the energy of the LUMO for the chosen ligand (L) increased to such a high extent that any reductions on the complex were rather ruthenium, bpy or pap targeted in the respective complexes **1**, [2](ClO₄)₂ and [3](ClO₄)₂ (LUMO compositions in **1**: 67% participation of Ru; [2](ClO₄)₂: 86% participation of bpy and [3](ClO₄)₂: 85% participation of pap) and thereby led to the decomposition of the complexes into unidentifiable products.

Electrochemistry and electronic structures: an experimental and theoretical case study

The bis-chelated diruthenium complexes **1**, [2](ClO₄)₂ and [3](ClO₄)₂ exhibited a series of successive electron transfer responses upon being screened with cyclic voltammetry and differential pulse voltammetry in acetonitrile within the accessible solvent window of ±2 V (Fig. 7 and Table 1).

As previously mentioned, complex **1** exists as a diastereomeric pair, **1a** (*rac*(ΔΔ/ΛΛ)) and **1b** (*meso*(ΔΛ)), which is not uncommon. However, it has been quite recurrently observed that such isomerism hardly impacts the electrochemical or electronic properties and the pair rather displays a similar behaviour, as can also be observed for **1a** and **1b**.¹⁶ The responses marked by * in Fig. 7(a and b) were observed repeatedly even after many attempts of purification. Their exact nature or origin cannot be authenticated and may be ascribed to some inherent electrode deposition for this set of complexes. Changing the scanning directions also had no impact on the * marked responses and the cyclic voltammograms for **1a** and **1b** were essentially the same as that of the equilibrium scan. Dicationic complex [2](ClO₄)₂ with a moderately π-accepting bipyridine terminal ligand shows multiple redox events which are shifted to more negative potentials in comparison with that of neutral **1** (for instance, the first redox events O1/R1 were observed for **1** at 1.11/−0.49 V and for [2]

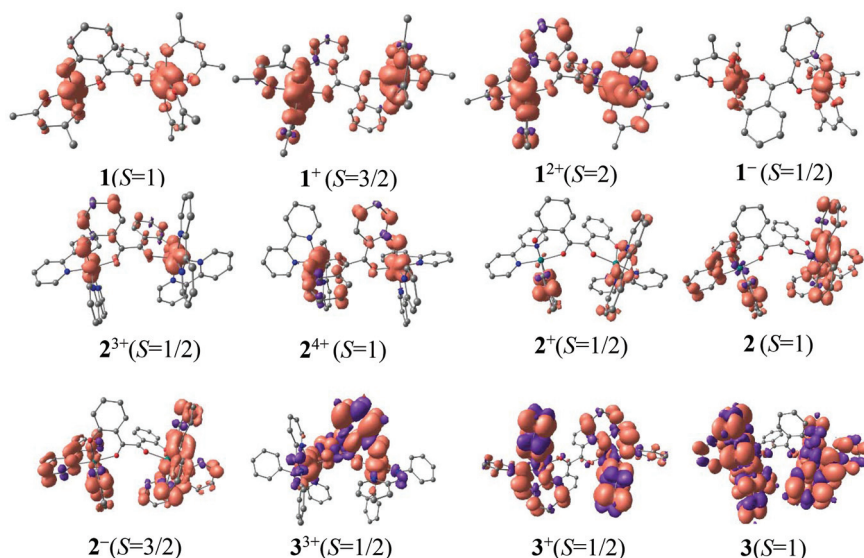


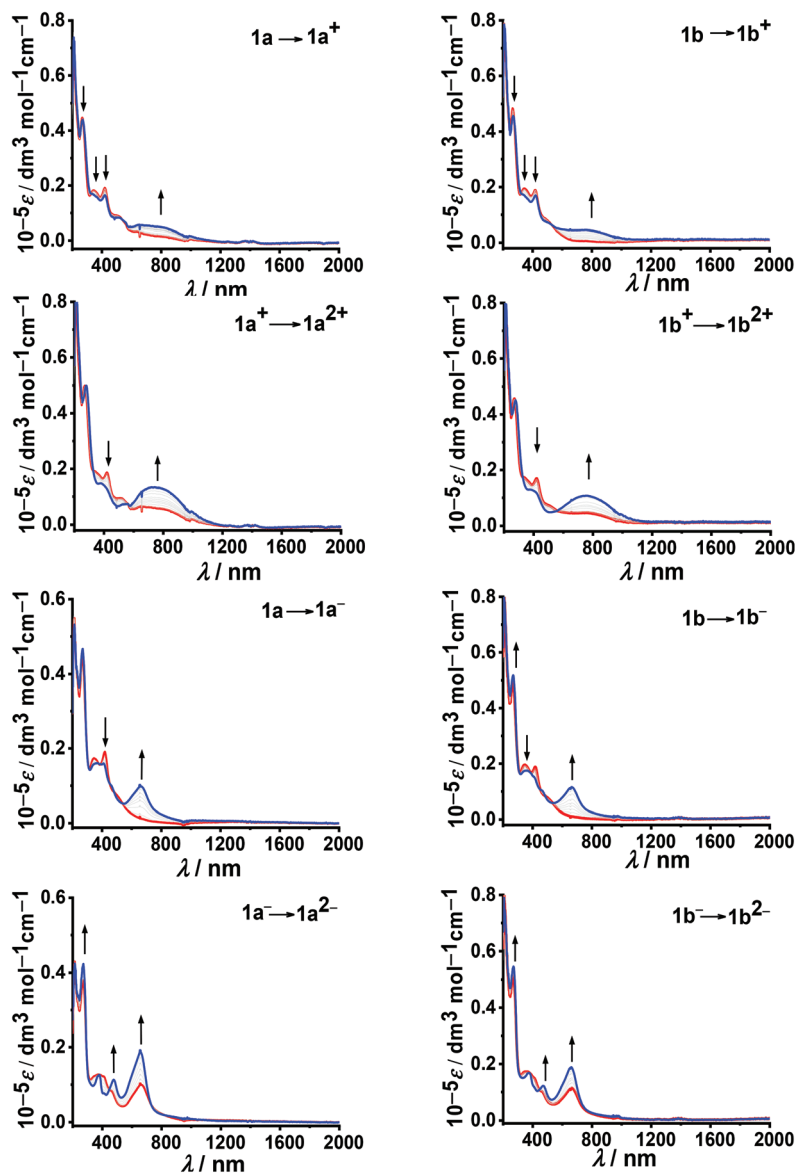
Fig. 8 Calculated Mulliken spin density plots for the various accessible redox states.

Table 2 DFT calculated (UB3LYP/LanL2DZ/6-31G*) Mulliken spin densities

Complex	Ru1	Ru2	L	acac ⁻	bpy	pap
1a ²⁺ (<i>S</i> = 2)	1.227	1.216	0.838	0.834	—	—
1a ⁺ (<i>S</i> = 3/2)	1.050	0.967	0.472	0.515	—	—
1a (<i>S</i> = 1)	0.801	0.802	0.200	0.200	—	—
1a ⁻ (<i>S</i> = 1/2)	0.354	0.505	0.071	0.075	—	—
2 ⁴⁺ (<i>S</i> = 1)	0.699	0.717	0.575	—	0.024	—
2 ³⁺ (<i>S</i> = 1/2)	0.272	0.322	0.424	—	-0.013	—
2 ⁺ (<i>S</i> = 1/2)	0.014	-0.003	0.004	—	1.027	—
2 (<i>S</i> = 1)	-0.031	-0.030	0.001	—	2.069	—
2 ⁻ (<i>S</i> = 3/2)	0.049	0.022	0.021	—	2.995	—
3 ³⁺ (<i>S</i> = 1/2)	0.222	0.222	0.614	—	—	-0.045
3 ⁺ (<i>S</i> = 1/2)	-0.042	-0.042	-0.002	—	—	1.081
3 (<i>S</i> = 1)	-0.178	-0.178	-0.018	—	—	2.224

(ClO₄)₂ at 0.71/−1.12 V, respectively). On the other hand, more positively shifted potentials were observed for dicationic complex [3](ClO₄)₂ containing a strongly π-accepting pap co-ligand with respect to that of bpy in [2](ClO₄)₂ (for instance, the first redox events O1/R1 were observed for [2](ClO₄)₂ at 0.71/−1.12 V and for [3](ClO₄)₂ at 1.49/−0.27 V, respectively). The shifts in the potentials upon moving from complex **1** to [2](ClO₄)₂ to [3](ClO₄)₂ may be attributed to an interplay between the differing metal oxidation states and the π-acidity of the changing ancillary ligands. The second oxidation for complex [3](ClO₄)₂ could not be perceived within the solvent window due to its probable anodic shift as an effect of the strong π-acidic nature of the pap ligands.

With these data in hand, attempts were made to explore the electronic distribution in varying accessible redox states (Scheme 2). In this context, considering together the Mulliken

**Fig. 9** UV-vis-NIR spectroelectrochemical response in CH₃CN/0.1 M nBu₄NPF₆ for **1**ⁿ.

spin density (MSD) and molecular orbital (MO) compositions obtained from the optimised molecular geometries for reversible redox states (Fig. 8, Table 2 and Tables S8–S22†) and EPR at the paramagnetic intermediate states (Fig. 3) we assigned the most suitable oxidation state scenarios. Due to similar experimental results of the diastereomeric pair **1a** and **1b**, the discussion shall be further continued considering the case of **1a**, for maintaining clarity. The EPR data for complex **1** can be interpreted in terms of a triplet state and a MSD of around 0.801 at each ruthenium centre suggests a Ru^{III}/Ru^{III} configuration in the native state ($E_{S=1} - E_{S=0} = 10\,360\text{ cm}^{-1}$, Table S23†). For the oxidised species **1a**⁺, no EPR response could be recorded, which is not too unlikely, due to the more stable but electronically complicated quartet state for the intermediate.^{10b} DFT calculated spin densities point towards a metal based oxidation (Ru^{III}/Ru^{IV}) with slight participation from the ligand (that contains electron rich phenoxyl groups) which is also corroborated by the MO composition of the SOMO having a significant ligand contribution (Ru/L/acac⁻: 0.23/0.54/0.23), suggestive of an alternately resonating electronic form (Ru^{III}/L⁻/Ru^{III}). A similar excited state ($E_{S=3/2} -$

$E_{S=1/2} = 285\text{ cm}^{-1}$, Table S23†) is suggestive of the presence of antiparallel spin alignment (up-up-down) in a three spin state configuration.¹⁸ For these complexes, the mixed valency through the mixed acceptor donor bridge may be an outcome of both the hole- and electron-transfer mechanisms operating simultaneously.¹⁶ The spin situation for **1a**²⁺ can also be rationalised as a resonating situation between Ru^{IV}/Ru^{IV} ↔ Ru^{III}/L⁻/Ru^{IV} ($S = 2$). Due to the presence of ruthenium centres in a relatively high valent oxidation state(III), the reductions are primarily metal centred and rather delocalised as may be inferred from the Mulliken spin density calculations. The comproportionation constant ($K_c = 10^3$) however suggests a more localised situation particularly from an electrochemical point of view.^{10b}

The closed-shell ($S = 0$) bipyridine complex [2](ClO₄)₂ (Ru^{II}/Ru^{II}) upon oxidation displays a metal based rhombic EPR spectrum (corresponding to the odd electron containing the Ru^{II}/Ru^{III} intermediate as the major form) which can be rationalised in terms of the competition between the increased electron density at the metal and the increased π -acceptor characteristic of the terminal ligand (with respect to the electron

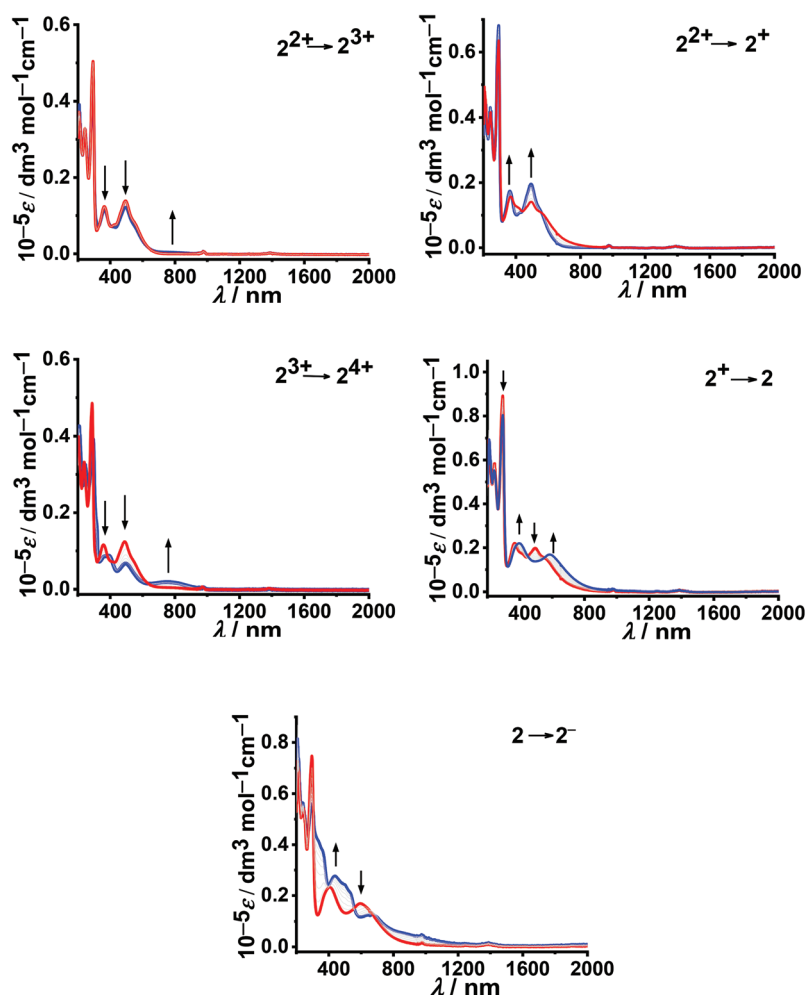


Fig. 10 UV-vis-NIR spectroelectrochemical response in CH₃CN/0.1 M *n*Bu₄NPF₆ for **2ⁿ**.

donating acetylacetonate ancillary ligand). However, the Mulliken spin density at the ligand may originate from a minor alternate ligand-bound radical containing intermediate as depicted in Scheme 2. The second oxidation leads to a delocalised radical bridged $\text{Ru}^{\text{II}+0.5}/\text{L}^-/\text{Ru}^{\text{II}+0.5}$ mixed valence state.^{12a} On the other hand, the electrogenerated species, 3^{3+} displays a clear ligand based EPR response with a g value of 2.000. The EPR spectra, Mulliken spin density and MO compositions unequivocally establish the reduction events on both the dicationic complexes (2^{2+} and 3^{2+}) to be co-ligand targeted (bipyridine and phenylazopyridine, respectively) as they possess suitable π -acceptor orbitals to receive the incoming electron density. It is interesting to note that the otherwise commonly reducible carbonyl groups in the diketo moiety remained unaltered upon reduction (*vide supra*). A second electron reduction of 3^{2+} led to a ligand based EPR with a triplet signal ($g_{1/2} = 3.972$) as is expected for the second electron to reduce another pap unit in **3** ($S = 1$).

UV-vis-NIR spectroelectrochemistry

Ultraviolet-visible-near-infrared (UV-vis-NIR) spectroelectrochemistry (Fig. 9–11 and Fig. S4a–c† (on the expanded scale for a clearer visible region)) along with the theoretical results assists in the assignment and authentication of oxidation state combinations at the accessible redox states (Scheme 2). The changing absorption characteristics of the complexes **1**, $[2](\text{ClO}_4)_2$ and $[3](\text{ClO}_4)_2$ were monitored through UV-vis-NIR spectroelectrochemistry using an optically transparent thin-layer electrochemical (OTTLE) cell at electrochemically reversible redox states with well defined isosbestic points. Attempts to assign the origins of these transitions have been made through time dependent density functional theory (TD-DFT) calculations (Table S24†). However, since each absorption band constitutes several closely lying transitions, the discussion is therefore based on the key transitions. Several mixed metal–ligand charge transfer transitions exist (Table S24†) primarily due to the inherent covalency factor¹⁹ arising out of the high spin–orbit coupling constant of ruthenium ($\text{Ru}(\lambda) = 1000 \text{ cm}^{-1}$ (ref. 4a and 16)).

The spectroscopic features and the following behaviour of the multiple redox states upon electrolysis of the diastereomeric complexes **1a/1b** were nearly identical in nature. **1a** in its native $\text{Ru}^{\text{III}}/\text{Ru}^{\text{III}}$ form exhibited ligand to metal charge transfer (LMCT) transitions in the high energy region. Mixed MLCT (metal to ligand charge transfer) and LMCT transitions were observed for both the one electron and two electron oxidised forms, $1a^+$ and $1a^{2+}$, respectively, and they may be originated from the resonating electronic configurations. Any significant increase in the intensity or a well defined absorption band in the low energy region, arising due to the mixed valency, could not be spotted, which is not uncommon for complexes with acetylacetonate peripheries.²⁰ The electronically reduced species $1a^-$ displayed many transitions which enveloped LMCT transitions in the visible region along with a very weak and broad increase in the intensity in the NIR region corresponding to the metal to metal charge transfer

(MMCT) transitions as an inter valence charge transfer (IVCT) band implicating the existence of a localised $\text{Ru}^{\text{II}}/\text{Ru}^{\text{III}}$ class II mixed valence situation. Further reduction on the complex led to the extinguishing of the weak and broad NIR band corresponding to the formation of an iso-valent diruthenim ($\text{Ru}^{\text{II}}/\text{Ru}^{\text{II}}$) species, $1a^{2-}$.

MLCT transitions targeted towards the ligand and moderately π -accepting bipyridine are observed for the dicationic complex, $[2](\text{ClO}_4)_2$. For these set of accessible redox states, no expected IVCT band in the NIR region was seen which could be interpreted in terms of weaker electronic coupling between the metals. Although this is less common a few examples similar to this situation have been documented in the literature.²¹ The successive oxidation processes display the expected MLCT transitions whereas the reductions are mainly assigned to the L/bpy targeted LMCT transitions.

Unlike $[2](\text{ClO}_4)_2$, the transitions in $[3](\text{ClO}_4)_2$ are MLCT transitions but solely to the π^* -orbital of the stronger π -acidic pap co-ligand. The one electron oxidised 3^{3+} , with ligand centred oxidation, revealed a strong low energy band at

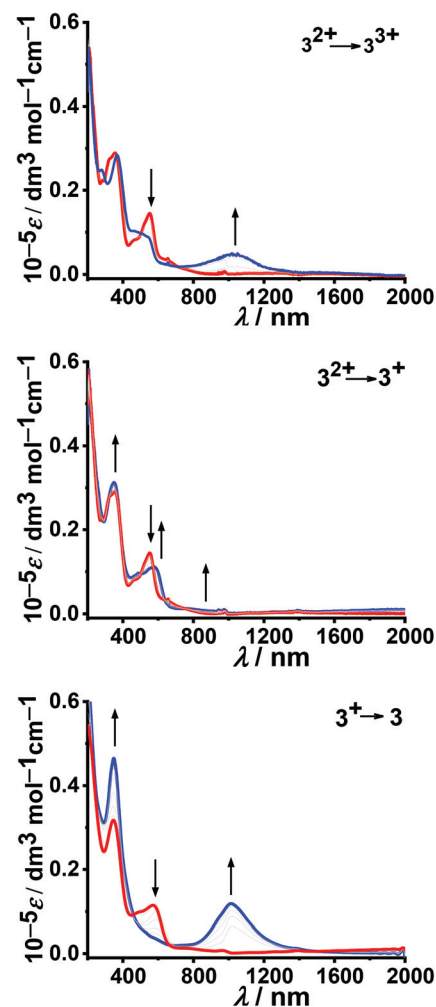


Fig. 11 UV-vis-NIR spectroelectrochemical response in $\text{CH}_3\text{CN}/0.1 \text{ M } n\text{Bu}_4\text{NPF}_6$ for 3^n .

1033 nm with underlying MLCT and intraligand (IL) transitions, largely targeted toward the oxidised ligand. Upon successive reductions in $[3](\text{ClO}_4)_2$, a weak and broad increment in the intensity is observed with the first reduction and it develops into a strong and sharp band at 1009 nm. These low energy bands mostly originate from IL transitions or mixed metal to ligand transitions. The visible range bands are of mixed MLCT or IL character but are pap targeted only.

Conclusion

Homometallic diruthenium complexes bridged by 1,2-bis(2-hydroxyphenyl)ethane-1,2-dione (L) have been probed for redox non-innocence and any reactivity resulting from the diketo fragment of the ligand. Conventional yet prototypical metal fragments consisting of co-ligands with differing electronic properties, $[\text{Ru}(\text{acac})_2]$, $[\text{Ru}(\text{bpy})_2]$ and $[\text{Ru}(\text{pap})_2]$ bis-chelated around the ligand, led to the formation of air stable **1a/1b**, $[2](\text{ClO}_4)_2$ and $[3](\text{ClO}_4)_2$, respectively. The following concluding remarks may be summed up from an extensive experimental and theoretical analysis of the complexes **1a/1b**, $[2](\text{ClO}_4)_2$ and $[3](\text{ClO}_4)_2$:

1. The chelating ligand containing a phenoxyl moiety actively participates in reversible oxidation processes and thereby leads to resonating redox state formalisms. Thereby, this redox active ligand can be unambiguously called as a redox non-innocent ligand in the context of these redox non-innocent compounds. However, the ligand contribution upon oxidation in each complex is not the same. It is rather a function of two factors: (i) the oxidation state of the metal and (ii) the different donating/accepting capacities of the co-ligands. The higher the oxidation state of the metal, the more would be the probability of the ligand to participate in the oxidation process. Whereas, the higher the π -accepting capability of the terminal ligand, the more would be the electron density of the metal drifting towards the ancillary ligand and hence the bridging ligand shall be available for a greater participation in the oxidation process. This observation of differing ligand contribution upon oxidation in the complexes **1a/1b**, $[2](\text{ClO}_4)_2$ and $[3](\text{ClO}_4)_2$ allows for the fine tuning of the redox potentials by changing the terminal ligand handles.

2. Though the diketo moiety has been previously reported to be fragile with respect to its sensitivity towards air,⁵ these set of complexes with a judiciously chosen ligand yield stable complexes. Thereby, with a slight re-designing or modification of the ligand framework, the molecular properties may be controlled to such an extent that a fragile and reactive site may be rendered stable.

These results are of fundamental interest as they extend the scope to investigate similar ligand frameworks in coordination compounds and check for their varying response towards stability/reactivity by changing the sterics and electronics in and around the ligand. Since many of the redox active complexes find place in biomimetic chemistry or even catalysis, more generalisations in this regard would be an added impetus.

Experimental section

Materials

The precursor complexes *cis*- $\text{Ru}(\text{acac})_2(\text{CH}_3\text{CN})_2$,²² *cis*- $\text{Ru}(\text{bpy})_2\text{Cl}_2$,²³ and *cis-trans-cis*- $\text{Ru}(\text{pap})_2\text{Cl}_2$ (ref. 24) were prepared by following a previously reported literature procedure. Oxalyl chloride and phenol were purchased from Sigma Aldrich. Phenol was added to a suspension of AlCl_3 in CH_2Cl_2 followed by the addition of oxalyl chloride to yield 1,2-bis(2-hydroxyphenyl)ethane-1,2-dione(L) following a reported literature procedure.²⁵ Other chemicals and solvents were of reagent grade and were used as received. For spectroscopic and electrochemical studies, HPLC grade solvents were used.

Physical measurements

The electrical conductivity of the solutions for the corresponding complexes **1**, $[2](\text{ClO}_4)_2$, $[3](\text{ClO}_4)_2$ was checked using an autoranging conductivity meter (Toshcon Industries, India). Cyclic voltammetric and differential pulse voltammetric measurements of the complexes were performed using a PAR model 273A electrochemistry system. A glassy carbon working electrode, platinum wire auxiliary electrode and saturated calomel reference electrode (SCE) were used in a standard three-electrode configuration with tetraethylammonium perchlorate (TEAP) as the supporting electrolyte (substrate concentration $\approx 10^{-3}$ M; standard scan rate 100 mV s^{-1}) (**Caution! Perchlorate salts are explosive and should be handled with care**). All electrochemical experiments were carried out under a dinitrogen atmosphere. The half wave potential E_{298}^o was set to $0.5(E_{\text{pa}} + E_{\text{pc}})$, where E_{pa} and E_{pc} are anodic and cathodic cyclic voltammetry peak potentials, respectively. The EPR measurements were performed in a two electrode capillary tube²⁶ with an X-band (9.5 GHz) Bruker system ESP300 spectrometer. UV-vis-NIR spectroelectrochemical studies were performed in $\text{CH}_3\text{CN}/0.1 \text{ M Bu}_4\text{NClO}_4$ at 298 K using an optically transparent thin-layer electrode (OTTLE) cell²⁷ mounted on the sample compartment of a J&M TIDAS spectrophotometer. ^1H NMR spectra were recorded on a Bruker Avance III 500 MHz spectrometer. The elemental analyses were performed using a PerkinElmer 240C elemental analyser. Electrospray mass spectral (ESI-MS) measurements were done using a Bruker's Maxis Impact (282001.00081) spectrometer.

Preparation of the complexes

Synthesis of $[(\text{acac})_2\text{Ru}^{\text{III}}(\mu\text{-L}^{2-})\text{Ru}^{\text{III}}(\text{acac})_2]$, **1a and **1b**.** The ligand L (31.75 mg, 0.13 mmol), the precursor *cis*- $\text{Ru}^{\text{II}}(\text{acac})_2(\text{CH}_3\text{CN})_2$ (100 mg, 0.26 mmol) and the base Et_3N (33 mg, 0.32 mmol) were refluxed in 20 cm^3 of toluene under a dinitrogen atmosphere for 5 h. The solvent was evaporated to dryness under reduced pressure and the solid mass was subjected to purification on a neutral alumina column, which eluted brown coloured products **1a** and **1b** with 1 : 2 and 1 : 4 pet ether : CH_2Cl_2 mixtures, respectively.

1a: yield, 50.54 mg, 46%. MS (ESI⁺, CH_3CN), m/z calcd for $\{\mathbf{1a}\}^+$: 840.03; found: 840.13. ^1H NMR (500 MHz, CDCl_3 , 298 K): δ (ppm, J (Hz)): 19.05 (d, 1H), 17.55 (s, 1H), 1.85 (t, 2H), 1.62 (m, 1H), 1.18 (d, 2H), 0.80(s, 2H), -3.91 (d, 5H), -10.28 (s,

1H), -17.92 (s, 2H), -26.15 (s, 1H). Λ_M ($\Omega^{-1} \text{ cm}^2 \text{ M}^{-1}$) in CH_3CN at 298 K = 3. Anal. calcd for $\text{C}_{34}\text{H}_{36}\text{O}_{12}\text{Ru}_2$: C, 48.68; H, 4.33; found: C, 48.75; H, 4.30.

1b: Yield, 39.56 mg, 36%. MS (ESI^+ , CH_3CN), m/z calcd for $\{\mathbf{1b}\}^+$: 840.03; found: 840.07. ^1H NMR (500 MHz, CDCl_3 , 298 K): δ (ppm, J (Hz)): 18.88 (s, 1H), 1.84 (m, 4H), 1.10 (m, 4H), -0.04 (s, 2H), -4.01 (s, 2H), -8.64(d, 1H), -12.51 (m, 2H), -17.65 (s, 1H), -26.36 (s, 1H). Λ_M ($\Omega^{-1} \text{ cm}^2 \text{ M}^{-1}$) in CH_3CN at 298 K = 7. Anal. calcd for $\text{C}_{34}\text{H}_{36}\text{O}_{12}\text{Ru}_2$: C, 48.68; H, 4.33; found: C, 48.76; H, 4.30.

Synthesis of $[(\text{bpy})_2\text{Ru}^{\text{II}}(\mu\text{-L}^{2-})\text{Ru}^{\text{II}}(\text{bpy})_2](\text{ClO}_4)_2$, $[\mathbf{2}](\text{ClO}_4)_2$. The precursor *cis*- $\text{Ru}(\text{bpy})_2\text{Cl}_2$ (100 mg, 0.21 mmol) and AgClO_4 (93 mg, 0.45 mmol) were added to 30 cm^3 of EtOH and heated to reflux for 2 h for dechlorination. The precipitated AgCl was removed by filtering the mixture using a sintered Gooch crucible. The filtrate was mixed with 20 cm^3 of a hot ethanolic solution of L (24.9 mg, 0.10 mmol) and Et_3N (31.36 mg, 0.3 mmol) and heated to reflux for 12 h under a dinitrogen atmosphere. The solvent was evaporated to dryness and the product was purified using a neutral alumina column, and the dark pink complex $[\mathbf{2}](\text{ClO}_4)_2$ was eluted with a CH_2Cl_2 : CH_3CN (3 : 1) solvent mixture.

$[\mathbf{2}](\text{ClO}_4)_2$: yield 91.69 mg, 70%. MS (ESI^+ , CH_3CN), m/z calcd for $\{\mathbf{2}(\text{ClO}_4)\}^+$: 1168.13; found 1168.16. ^1H NMR (500 MHz, CD_3CN , 298 K): δ (ppm, J (Hz)): 8.95 (d, 2H), 8.84 (d, 2H), 8.65 (d, 2H), 8.64 (d, 2H), 8.57 (d, 2H), 8.43(d, 2H), 8.29 (t, 2H), 8.18 (t, 2H), 7.91 (m, 3H), 7.82 (d, 3H), 7.77 (t, 2H), 7.71 (t, 1H), 7.49(t, 2H), 7.26 (m, 3H), 7.16 (t, 2H), 7.12 (d, 1H), 6.92 (d, 2H), 6.73 (t, 3H), 6.67 (t, 1H), 6.38 (s, 1H). Λ_M ($\Omega^{-1} \text{ cm}^2 \text{ M}^{-1}$) in CH_3CN at 298 K = 262. Anal. calcd for $\text{C}_{54}\text{H}_{40}\text{O}_{12}\text{N}_8\text{Ru}_2\text{Cl}_2$: C, 51.23; H, 3.18; N, 8.85; found: C, 51.51; H, 3.30; N, 8.98.

Synthesis of $[(\text{pap})_2\text{Ru}^{\text{II}}(\mu\text{-L}^{2-})\text{Ru}^{\text{II}}(\text{pap})_2](\text{ClO}_4)_2$, $[\mathbf{3}](\text{ClO}_4)_2$. Complex $[\mathbf{3}](\text{ClO}_4)_2$ was synthesised by following the similar protocol to $[\mathbf{2}](\text{ClO}_4)_2$. The precursor *cis-trans-cis*- $\text{Ru}(\text{pap})_2\text{Cl}_2$ (100 mg, 0.19 mmol) was dechlorinated with AgClO_4 (83 mg, 0.40 mmol) in 30 cm^3 of EtOH under reflux for 2 h. The precipitated AgCl was filtered off using a sintered Gooch crucible. The filtrate was added to 20 cm^3 of a hot ethanolic solution of the ligand L (34 mg, 0.095 mmol) and base Et_3N (20 mg, 0.20 mmol) and refluxed under a dinitrogen atmosphere for 12 h. Post removal of the solvent under vacuum, the reaction mixture was chromatographed on a neutral alumina column. The pink compound $[\mathbf{3}](\text{ClO}_4)_2$ was eluted with a CH_2Cl_2 : CH_3CN (2 : 1) solvent mixture.

$[\mathbf{3}](\text{ClO}_4)_2$: yield 85.2 mg (67%). MS (ESI^+ , CH_3CN), m/z calcd for $\{\mathbf{3}(\text{ClO}_4)\}^+$: 1274.10; found 1274.07. ^1H NMR (500 MHz, $(\text{CD}_3)_2\text{SO}$, 298 K): δ (ppm, J (Hz)): 9.08 (m, 1H), 9.02 (m, 1H), 8.47 (m, 2H), 8.10 (m, 1H), 7.78 (t, 1H), 7.71(t, 1H), 7.63 (d, 1H), 7.49 (q, 3H), 7.32 (m, 6H), 6.89 (d, 2H), 6.77 (d, 1H), 6.69 (m, 1H), 6.59(d, 1H). Λ_M ($\Omega^{-1} \text{ cm}^2 \text{ M}^{-1}$) in CH_3CN at 298 K = 230. Anal. calcd for $\text{C}_{58}\text{H}_{44}\text{O}_{12}\text{N}_{12}\text{Ru}_2\text{Cl}_2$: C, 50.70; H, 3.23; N, 12.23; found: C, 50.95; H, 3.29; N, 12.41.

Crystal structure determination

Single crystals were obtained by slow evaporation of the 1 : 1 solution of CH_2Cl_2 - CH_3CN and the 1 : 1 : 1 solution of

CH_3OH - CH_3CN - C_6H_6 for $[\mathbf{2}](\text{ClO}_4)_2$ and $[\mathbf{3}](\text{ClO}_4)_2$, respectively. X-ray diffraction data were collected using a Rigaku Saturn-724 + CCD single crystal diffractometer using $\text{Mo-K}\alpha$ radiation. The data collection was evaluated by using the CrystalClear-SM Expert software. The data were collected by the standard ω -scan technique. The structure was solved by direct methods using SHELXT-2015a and refined by full matrix least-squares with SHELXL-2018/3 on F^2 .²⁸ All data were corrected for Lorentz and polarization effects and all non-hydrogen atoms were refined anisotropically. The remaining hydrogen atoms were placed in the geometrically constrained positions and refined with isotropic temperature factors, generally $1.2U_{\text{eq}}$ of their parent atoms. The hydrogen atoms were included in the refinement process as per the riding model. The disordered groups in $[\mathbf{2}](\text{ClO}_4)_2$ and $[\mathbf{3}](\text{ClO}_4)_2$ were modelled using the PART command. In addition to the benzene solvate molecule that can be seen in the data of $[\mathbf{2}](\text{ClO}_4)_2$, there are two other benzene solvent molecules present. However they are both disordered and removed by applying SQUEEZE using the PLATON package to achieve better convergence.²⁹ The Cambridge Crystallographic Data Centre has provided the CCDC numbers 2026821 and 2026822 for $[\mathbf{2}](\text{ClO}_4)_2$ and $[\mathbf{3}](\text{ClO}_4)_2$, respectively.†

Computational details

Full geometry optimisations were carried out using the density functional theory method at the (U)B3LYP level for $\mathbf{1a}^n/\mathbf{1b}^n$ ($n = 2+$, $1+$, 0 , $1-$), $\mathbf{2}^n$ ($n = 4+$, $3+$, $1+$, 0 , $1-$), $\mathbf{3}^n$ ($n = 3+$, $1+$, 0) and (R)B3LYP for $\mathbf{1a}^n/\mathbf{1b}^n$ ($n = 2-$), $\mathbf{2}^n$ ($n = 2+$), $\mathbf{3}^n$ ($n = 2+$).³⁰ All elements except ruthenium were assigned to the 6-31G(d) basis set. The LanL2DZ basis set with effective core potential was employed for the ruthenium atom.³¹ All calculations were performed with the Gaussian09 program package.³² Vertical electronic excitation based on the (U)B3LYP optimised geometries was computed using the time-dependent density functional theory (TD-DFT) formalism³³ in acetonitrile using the conductor-like polarizable continuum model (CPCM).³⁴ Chemission 1.7³⁵ was used to calculate the fractional contributions of various groups to each molecular orbital. All calculated structures were visualised with ChemCraft.³⁶

Conflicts of interest

The authors declare no competing financial interest.

Acknowledgements

Financial support received from the Science and Engineering Research Board (SERB, DST), the J. C. Bose Fellowship (to G. K. L., SERB), New Delhi, India, DAAD-Germany and IIT Bombay (fellowship to F. F. K.) is gratefully acknowledged. Prof. R. J. Butcher, Department of Chemistry, Howard University, USA, is also gratefully acknowledged for his help in solving the crystal structures of $[\mathbf{2}](\text{ClO}_4)_2$ and $[\mathbf{3}](\text{ClO}_4)_2$.

References

- 1 (a) S. H. Light, L. Su, R. Rivera-Lugo, J. A. Cornejo, A. Louie, A. T. Iavarone, C. M. Ajo-Franklin and D. A. Portnoy, *Nature*, 2018, **562**, 140–144; (b) J. Madeo, A. Zubair and F. Marianne, *SpringerPlus*, 2013, **2**, 1–8; (c) A. Alsiyabi, C. M. Immethun and R. Saha, *Sci. Rep.*, 2019, **9**, 1–9; (d) Y. Qin, L. Zhang, J. Lv, S. Luo and J.-P. Cheng, *Org. Lett.*, 2015, **17**, 1469–1472.
- 2 F. F. Khan, A. D. Chowdhury and G. K. Lahiri, *Eur. J. Inorg. Chem.*, 2020, **2020**, 1138–1146.
- 3 (a) M. Fontecave and J.-L. Pierre, *Coord. Chem. Rev.*, 1998, **170**, 125–140; (b) C. Belle and J.-L. Pierre, *Eur. J. Inorg. Chem.*, 2003, **2003**, 4137–4146; (c) J. P. Klinman and F. Bonnot, *Chem. Rev.*, 2014, **114**, 4343–4365; (d) M. Mure, *Acc. Chem. Res.*, 2004, **37**, 131–139.
- 4 (a) W. Kaim and G. K. Lahiri, *Coord. Chem. Rev.*, 2019, **393**, 1–8; (b) M. A. Ansari, K. Beyer, A. Paretzki, J. Fiedler, W. Kaim and G. K. Lahiri, *Chem. – Asian J.*, 2018, **13**, 2947–2965; (c) A. Mandal, A. Grupp, B. Schwederski, W. Kaim and G. K. Lahiri, *Inorg. Chem.*, 2015, **54**, 7936–7944; (d) T. Kundu, B. Sarkar, T. K. Mondal, S. M. Mobin, F. A. Urbanos, J. Fiedler, R. Jiménez-Aparicio, W. Kaim and G. K. Lahiri, *Inorg. Chem.*, 2011, **50**, 4753–4763; (e) D. Kumbhakar, B. Sarkar, S. Maji, S. M. Mobin, J. Fiedler, F. A. Urbanos, R. Jiménez-Aparicio, W. Kaim and G. K. Lahiri, *J. Am. Chem. Soc.*, 2008, **130**, 17575–17583; (f) A. Lutch, S. Sobottka, L. J. Patalag, P. G. Jones, H.-U. Reissig, B. Sarkar and D. B. Werz, *Chem. – Eur. J.*, 2019, **25**, 10359–10365; (g) U. Albold, C. Hoyer, N. I. Neuman, S. Sobottka, A. S. Hazari, G. K. Lahiri and B. Sarkar, *Inorg. Chem.*, 2019, **58**, 3754–3763.
- 5 F. F. Khan, S. Sobottka, B. Sarkar and G. K. Lahiri, *Chem. – Eur. J.*, 2019, **25**, 9737–9746.
- 6 M.-S. Seo, A. Lee and H. Kim, *Org. Lett.*, 2014, **16**, 2950–2953.
- 7 M. K. Biswas, S. C. Patra, A. N. Maity, S.-C. Ke, T. Weyhermuller and P. Ghosh, *Chem. Commun.*, 2013, **49**, 4522–4524.
- 8 (a) D. Samanta, P. Saha and P. Ghosh, *Inorg. Chem.*, 2019, **58**, 15060–15077; (b) M. Orio, O. Jarjayes, B. Baptiste, C. Philouze, C. Duboc, J. L. Mathias, L. Benisvy and F. Thomas, *Chem. – Eur. J.*, 2012, **18**, 5416–5429; (c) W. Kaim, *Dalton Trans.*, 2003, 761–768; (d) E. R. Altwicker, *Chem. Rev.*, 1967, **67**, 475–531.
- 9 (a) S. Patra, B. Sarkar, S. Maji, J. Fiedler, F. A. Urbanos, R. Jiménez-Aparicio, W. Kaim and G. K. Lahiri, *Chem. – Eur. J.*, 2006, **12**, 489–498; (b) Y. Wang, J. L. DuBois, B. Hedman, K. O. Hodgson and T. D. P. Stack, *Science*, 1998, **279**, 537–540; (c) S. Itoh, M. Taki and S. Fukuzumi, *Coord. Chem. Rev.*, 2000, **198**, 3–20.
- 10 (a) P. Mondal, M. Chatterjee, A. Paretzki, K. Beyer, W. Kaim and G. K. Lahiri, *Inorg. Chem.*, 2016, **55**, 3105–3116; (b) F. F. Khan, J. Klein, J. L. Priego, R. Jimenez-Aparicio, B. Sarkar and G. K. Lahiri, *Inorg. Chem.*, 2018, **57**, 12800–12810.
- 11 (a) F. F. Khan, A. Mandal, J. Klein, J. L. Priego, R. Jiménez-Aparicio, B. Sarkar and G. K. Lahiri, *Eur. J. Inorg. Chem.*, 2017, 5497–5506; (b) M. Chatterjee, P. Ghosh, K. Beyer, A. Paretzki, J. Fiedler, W. Kaim and G. K. Lahiri, *Chem. – Asian J.*, 2018, **13**, 118–125.
- 12 (a) M. A. Ansari, A. Mandal, A. Paretzki, K. Beyer, J. Fiedler, W. Kaim and G. K. Lahiri, *Inorg. Chem.*, 2016, **55**, 5655–5670; (b) A. Mandal, H. Agarwala, R. Ray, S. Plebst, S. M. Mobin, J. L. Priego, R. Jimenez-Aparicio, W. Kaim and G. K. Lahiri, *Inorg. Chem.*, 2014, **53**, 6082–6093.
- 13 (a) S. Ghumaan, B. Sarkar, S. Patra, J. van Slageren, J. Fiedler, W. Kaim and G. K. Lahiri, *Inorg. Chem.*, 2005, **44**, 3210–3214; (b) R. S. Drago, in *Physical Methods for Chemists*, Saunders College Publishing, New York, 2nd edn, 1992, pp. 390; (c) S. Kar, B. Sarkar, S. Ghumaan, D. Janardanan, J. van Slageren, J. Fiedler, V. G. Puranik, R. B. Sunoj, W. Kaim and G. K. Lahiri, *Chem. – Eur. J.*, 2005, **11**, 4901–4911.
- 14 (a) A. Mandal, A. Grupp, B. Schwederski, W. Kaim and G. K. Lahiri, *Inorg. Chem.*, 2015, **54**, 10049–10057; (b) P. Mondal, R. Ray, A. Das and G. K. Lahiri, *Inorg. Chem.*, 2015, **54**, 3012–3021.
- 15 M. Chatterjee, S. Mondal, P. Ghosh, W. Kaim and G. K. Lahiri, *Inorg. Chem.*, 2018, **57**, 12187–12194.
- 16 W. Kaim and G. K. Lahiri, *Angew. Chem., Int. Ed.*, 2007, **46**, 1778–1796.
- 17 C. Creutz, *Prog. Inorg. Chem.*, 1983, **30**, 1–73.
- 18 D. Kumbhakar, B. Sarkar, S. Maji, S. M. Mobin, J. Fiedler, F. A. Urbanos, R. Jimenez-Aparicio, W. Kaim and G. K. Lahiri, *J. Am. Chem. Soc.*, 2008, **130**, 17575–17583.
- 19 (a) W. Kaim, A. Das, J. Fiedler, S. Zalis and B. Sarkar, *Coord. Chem. Rev.*, 2020, **404**, 1–6; (b) D. Kalinina, C. Dares, P. Kaluarachchi, P. G. Potvin and A. B. P. Lever, *Inorg. Chem.*, 2008, **47**, 10110–10126; (c) J. Rusanova, E. Rusanova, S. I. Gorelsky, D. Christendat, R. Popescu, A. A. Farah, R. Beaulac, C. Reber and A. B. P. Lever, *Inorg. Chem.*, 2006, **45**, 6246–6262; (d) R. A. Metcalfe, L. C. G. Vasconcellos, H. Mirza, D. W. Franco and A. B. P. Lever, *J. Chem. Soc., Dalton Trans.*, 1999, 2653–2667.
- 20 (a) S. Patra, B. Sarkar, S. Ghumaan, J. Fiedler, W. Kaim and G. K. Lahiri, *Dalton Trans.*, 2004, 754–758; (b) S. Patra, B. Sarkar, S. Ghumaan, J. Fiedler, W. Kaim and G. K. Lahiri, *Inorg. Chem.*, 2004, **43**, 6108–6113.
- 21 (a) S. Patra, B. Sarkar, S. Maji, J. Fiedler, F. A. Urbanos, R. Jimenez-Aparicio, W. Kaim and G. K. Lahiri, *Chem. – Eur. J.*, 2006, **12**, 489–498; (b) W. Kaim, A. Klein and M. Glöckle, *Acc. Chem. Res.*, 2000, **33**, 755–763; (c) J. Poppe, M. Moscherosch and W. Kaim, *Inorg. Chem.*, 1993, **32**, 2640–2643; (d) M. D. Ward, *Inorg. Chem.*, 1996, **35**, 1712–1714.
- 22 T. Kobayashi, Y. Nishina, K. G. Shimizu and G. P. Satô, *Chem. Lett.*, 1988, **17**, 1137–1140.
- 23 B. P. Sullivan, D. J. Salmon and T. J. Meyer, *Inorg. Chem.*, 1978, **17**, 3334–3341.
- 24 S. Goswami and A. R. Chakravarty, *Inorg. Chem.*, 1983, **22**, 602–609.

- 25 M.-S. Seo, D. Sun and H. Kim, *J. Org. Chem.*, 2017, **82**, 6586–6591.
- 26 W. Kaim, S. Ernst and V. Kasack, *J. Am. Chem. Soc.*, 1990, **112**, 173–178.
- 27 M. Krejciak, M. Danek and F. Hartl, *J. Electroanal. Chem.*, 1991, **317**, 179–187.
- 28 (a) G. M. Sheldrick, *Acta Crystallogr., Sect. A: Found. Crystallogr.*, 2008, **64**, 112–122; (b) G. M. Sheldrick, *Program for Crystal Structure Solution and Refinement*, University of Göttingen, Göttingen, Germany, 1997.
- 29 P. van der Sluis and A. L. Spek, *Acta Crystallogr., Sect. A: Found. Crystallogr.*, 1990, **46**, 194–201.
- 30 C. Lee, W. Yang and R. G. Parr, *Phys. Rev. B: Condens. Matter Mater. Phys.*, 1988, **37**, 785–789.
- 31 (a) D. Andrae, U. Haeussermann, M. Dolg, H. Stoll and H. Preuss, *Theor. Chim. Acta*, 1990, **77**, 123–141; (b) P. Fuentealba, H. Preuss, H. Stoll and L. von Szentpaly, *Chem. Phys. Lett.*, 1989, **89**, 418–422.
- 32 M. J. Frisch, G. W. Trucks, H. B. Schlegel, G. E. Scuseria, M. A. Robb, J. R. Cheeseman, G. Scalmani, V. Barone, B. Mennucci, G. A. Petersson, H. Nakatsuji, M. Caricato, X. Li, H. P. Hratchian, A. F. Izmaylov, J. Bloino, G. Zheng, J. L. Sonnenberg, M. Hada, M. Ehara, K. Toyota, R. Fukuda, J. Hasegawa, M. Ishida, T. Nakajima, Y. Honda, O. Kitao, H. Nakai, T. Vreven, J. A. Montgomery Jr., J. E. Peralta, F. Ogliaro, M. Bearpark, J. J. Heyd, E. Brothers, K. N. Kudin, V. N. Staroverov, R. Kobayashi, J. Normand, K. Raghavachari, A. Rendell, J. C. Burant, S. S. Iyengar, J. Tomasi, M. Cossi, N. Rega, J. M. Millam, M. Klene, J. E. Knox, J. B. Cross, V. Bakken, C. Adamo, J. Jaramillo, R. Gomperts, R. E. Stratmann, O. Yazyev, A. J. Austin, R. Cammi, C. Pomelli, J. W. Ochterski, R. L. Martin, K. Morokuma, V. G. Zakrzewski, G. A. Voth, P. Salvador, J. J. Dannenberg, S. Dapprich, A. D. Daniels, O. Farkas, J. B. Foresman, J. V. Ortiz, J. Cioslowski and D. J. Fox, *Gaussian09 (Revision A.02)*, Gaussian, Inc., Wallingford CT, 2009.
- 33 (a) R. Bauernschmitt and R. Ahlrichs, *Chem. Phys. Lett.*, 1996, **256**, 454–464; (b) R. E. Stratmann, G. E. Scuseria and M. J. Frisch, *J. Chem. Phys.*, 1998, **109**, 8218–8225; (c) M. E. Casida, C. Jamorski, K. C. Casida and D. R. Salahub, *J. Chem. Phys.*, 1998, **108**, 4439–4450.
- 34 (a) V. Barone and M. Cossi, *J. Phys. Chem. A*, 1998, **102**, 1995–2001; (b) M. Cossi and V. Barone, *J. Chem. Phys.*, 2001, **115**, 4708–4718; (c) M. Cossi, N. Rega, G. Scalmani and V. Barone, *J. Comput. Chem.*, 2003, **24**, 669–681.
- 35 S. Leonid, *Chemissian 1.7*, 2005–2010, available at <http://www.chemissian.com>.
- 36 D. A. Zhurko and G. A. Zhurko, *ChemCraft 1.5*, Plimus, San Diego, CA, available at <http://www.chemcraftprog.com>.